

Scaling relations in charge and spin excitations for $\text{La}_{1-x}\text{Sr}_x\text{MnO}_3$

Nobuo Furukawa

*Institute for Solid State Physics, University of Tokyo, Minato-ku, Tokyo 106-8666, Japan,
and*

Institute for Theoretical Physics, ETH-Hönggerberg, CH-8093 Zurich, Switzerland

Yutaka Moritomo

Center for Integrated Research in Science and Engineering (CIRSE),

Nagoya Univ., Nagoya 464-8601 Japan

and

Precursory Research for Embryonic Science and Technology (PRESTO),

Japan Science and Technology Cooperation (JST), Chiyoda-ku, Tokyo 102, Japan

K. Hirota and Y. Endoh

Department of Physics, Tohoku University,

Aramaki Aoba, Sendai 980-77, Japan

(October 1, 2018)

Scaling relations in the charge and spin excitations of $\text{La}_{1-x}\text{Sr}_x\text{MnO}_3$ are studied from both theoretical and experimental points of view. In the ferromagnetic metal phase, we investigate optical conductivity and neutron inelastic scattering, and compare with a theoretical calculation based on the dynamical mean-field theory of the double-exchange hamiltonian. Spin and charge dynamics of $\text{La}_{1-x}\text{Sr}_x\text{MnO}_3$ exhibit typical behaviors of half metals. In these manganite compounds with high Curie temperature, various behaviors in spin and charge properties are explained by the double-exchange hamiltonian alone. Magnetoresistance of these compounds as well as other compounds with lower Curie temperature are also discussed.

I. INTRODUCTION

One of the main issues in colossal magnetoresistance (CMR) manganites (R,A) MnO_3 is to investigate how to control the electronic properties, especially these for transports, through magnetic field. In order to explain the ferromagnetism, Zener¹ introduced a model hamiltonian

$$\mathcal{H} = - \sum_{ij,\sigma} t_{ij} \left(c_{i\sigma}^\dagger c_{j\sigma} + h.c. \right) - J_H \sum_i \vec{\sigma}_i \cdot \vec{S}_i, \quad (1.1)$$

where t is the electron hopping energy and J_H is Hund's coupling between itinerant electron and localized spins, and proposed the double-exchange (DE) mechanism. Anderson and Hasegawa² took the infinite J_H limit of the model to discuss the ground state spin structure. However, at finite temperature, relationship between magnetism and electronic structure is not fully understood through these calculations. In the strong Hund's coupling limit $J_H \gg t$, mean-field theories which do not take into account effects of local spin fluctuations and neglect changes in electronic structure and lifetime of conducting

quasiparticles are not sufficient to understand thermodynamic properties including the Curie temperature T_c as well as resistivity. Therefore, a controlled method beyond the mean-field theory is necessary.

From the experimental point of view, recent improvements in precise control of the A-site cation substitutions revealed a complex phase diagram as a function of substitution, temperature and magnetic field, with various phases which exhibit magnetic, charge, orbital and lattice orderings.³ Although the DE hamiltonian can describe an antiferromagnet at half-filling and ferromagnetic metal at doped cases, it is clear that the model has to be extended in order to account for charge and orbital orderings. Theoretically, investigations are performed on several microscopic models, especially emphasis on polaronic models, to reproduce varieties of phases with different behaviors in resistivity and phase transitions.⁴ However, due to such a complexity with variety of phases, there is no satisfactory theory so far to explain properties in the entire parameter region of substitutions and temperature.

Another point of view is to discuss magnetoresistance (MR) of manganites in relation with other materials such as CrO_2 or $\text{Tl}_2\text{Mn}_2\text{O}_7$.⁵ Especially, in various ferromagnetic metals, the half-metallic behavior due to DE interaction is considered to cause so-called tunneling magnetoresistance (TMR) through the spin valve mechanism.⁶ Magnetoresistance of the material with artificially controlled grain/interface boundaries are also studied to realize a low-field MR device through TMR.⁷⁻⁹

Thus it is now important to discuss MR in manganites from the point of view of making distinction between generic DE half-metal properties and specific behaviors of these compounds. In this paper, we focus on the bulk nature of the DE systems in the ferromagnetic metal state. We study series of compounds which show the metallic ferromagnetism at the ground state, a canonical examples of which are $\text{La}_{1-x}\text{Sr}_x\text{MnO}_3$ with carrier density

$x = 0.2 \sim 0.4$, so-called ‘high- T_c ’ compounds, and compare with the theoretical results obtained from the DE hamiltonian. Investigations are through its charge and spin excitation properties. We present a comprehensive study by putting together theoretical and experimental results which have been described only briefly in previous short papers and letters by the authors, and provide a unified picture of the charge and the spin excitation spectra through the electronic structure of the half-metallic DE system. One of our aim is to establish the relevance of the half-metallic picture for the conduction electrons in these materials, and investigate the consequence of such a electronic structure to spin and charge dynamics through the DE mechanism. We also discuss MR of the low- T_c compounds such as $\text{La}_{2/3}\text{Ca}_{1/3}\text{MnO}_3$. In §2, we show theoretical results for DE Hamiltonian studied in a nonperturbative manner using the dynamical mean-field approach.^{10–13} In §3, we show experimental results for spin wave lifetime with respect to relatively high T_c samples of $((\text{La},\text{Y}),\text{Sr})\text{MnO}_3$.¹⁴ In §4, we show experimental results for optical spectrum for $(\text{La},\text{Sr})\text{MnO}_3$ as well as Nd substituted low T_c materials.¹⁵ Section 5 is devoted for discussion and summary.

II. THEORETICAL CALCULATION

A. Model and method

We consider a DE hamiltonian (1.1) which is now also called as ferromagnetic Kondo lattice model. Since we consider the case where the localized spin is in a high-spin state and the coupling to itinerant electrons is ferromagnetic due to Hund’s rule, the effect of quantum exchange is speculated to be irrelevant. Especially, near the Curie temperature T_c thermal fluctuations should be dominant. Thus we make an approximation to replace the quantum spins operators by classical rotators ($S = \infty$ limit), namely we replace the spin operators \vec{S}_i in (1.1) by classical fields with norm $|\vec{S}_i| = 1$.

We introduce the dynamical mean-field (DMF) method for the above system. Within this method, the system is treated by a single site interacting with an electronic bath, or the single particle Green’s function \tilde{G}_0 , which plays a role of a frequency-dependent Weiss field.¹⁶ In the limit $S = \infty$ where dynamics of the spin in the imaginary-time axis does not exist, the single-site problem is exactly solved albeit the problem must be solved self-consistently with respect to the external bath. For details, readers are referred to ref. 10.

Advantages of applying this method are: (i) Thermal fluctuations of localized spins are taken into account in a non-perturbative way. Finite temperature calculation in the thermodynamic limit is possible. (ii) Unlike the case for the Hubbard model^{16,17} the single-site problem is solved easily so that no additional approximation is

necessary. The problem is solved in either imaginary frequencies or real frequencies, so that electronic dynamics are obtained directly.

B. Results

1. Electronic Density of States and Half-Metallic Behaviors

In Fig. 1 we show the electron DOS $A_\sigma(\omega)$ in DMF on Bethe lattice at $J_H/W = 2$ and $x = 0.2$ which gives ferromagnetic ground state. We set the magnetization to be $+z$ direction. Results are qualitatively the same as long as the strong Hund’s coupling region with ferromagnetic ground state is concerned.

In the ground state with ferromagnetic ordering for the localized spins, Hund’s coupling splits the electron DOS into upper and lower subbands at $\omega = \pm J_H$, corresponding to the state parallel and anti-parallel to the ferromagnetically-ordered local spins. The width of the each DOS is the bandwidth of the noninteracting system. Therefore, in the case $2J_H > W$ where Zeeman splitting is larger than the bandwidth, we have a gap in DOS. The conduction band is half metallic, namely the Fermi surface exists only in one of the spin species.

In this system, the origin of the half-metallic behavior is due to large Hund’s coupling $J_H \gg W$. This state is in large contrast with itinerant weak ferromagnet which has smaller split of DOS and the Fermi surfaces in both spin species. In manganites with ferromagnetic metal state, half-metallic behaviors are observed in various experiments including photoemission,¹⁸ tunneling junction⁷ and grain boundary TMR measurements.⁶

At finite temperature, the spectra change in such a way that there exist two peaks at $\omega \sim \pm J_H$ and its integrated weight transfers by magnetization. The center of the both peaks split by J_H are roughly unchanged. Both spin species have finite weight in lower and upper subbands. For the occupied lower subband, integrated weight scales as $(1 + M^*)/2$ and $(1 - M^*)/2$ for up (parallel) and down (antiparallel) bands, respectively, where $M^* = \langle S_z \rangle / S$ is the magnetization of the local spin. Due to particle-hole symmetry, the upper subband have the weight $(1 - M^*)/2$ and $(1 + M^*)/2$ for up and down electrons, respectively. The width of each sub-bands changes in the way that at higher temperature the bandwidth is reduced due to smaller hopping matrix element.

This is easily understood, since the integrated weight of each subbands gives the spin polarization of the itinerant electron part, and in the strong Hund’s coupling limit it should be proportional to the spin polarization of the localized spin. The bandwidth of each subband becomes narrower than that for the ground state, which is understood from the reduction of the hopping matrix element.²

Above T_c , the DOS is still split into two bands, with the identical weight for both subbands in each spin species.

Within our approach, there is no temperature dependence above T_c . This is an artifact of the single-site approximation where spin correlation of finite length is not taken into account. However, for strong Hund's coupling, we speculate that the overall spectrum shape which is split into two subbands do not change by finite size cluster corrections.

To investigate the Majority-minority bands more precisely, Green's function is calculated as follows. From the solution of the DMF at $J_H/W \gg 1$ on a Lorentzian DOS system,¹² we have the analytical form for the self-energy

$$\Sigma_\sigma(\omega) = -J_H - \frac{1 - M\sigma}{1 + M\sigma}(\omega + \mu + J_H + iW) \quad (2.1)$$

at the lower subband $\omega \sim -J_H$ and $\sigma = \pm 1$. We also see a similar M dependence of Σ in semicircular DOS. Then, the lattice Green's function is given in the form

$$G(k, \omega) = \frac{z_\sigma(M)}{\omega - \zeta_{k, \sigma} + i\Gamma_\sigma} \quad (2.2)$$

where

$$\zeta_{k\sigma}(M) = \frac{1 + M\sigma}{2}\varepsilon_k - J_H - \mu, \quad (2.3)$$

$$z_\sigma(M) = \frac{1 - M\sigma}{2}, \quad (2.4)$$

$$\Gamma_\sigma(M) = \frac{1 + M\sigma}{2}W. \quad (2.5)$$

Since spin-dependent DOS is proportional to $z_\sigma(M)$, we see the relation $A_\uparrow(\omega) \propto (1 + M)/2$ and $A_\downarrow(\omega) \propto (1 - M)/2$.

Let us discuss the low temperature limit $1 - M \sim 0$. For the majority band, we recover the free-fermion behavior $z = 1$, $\zeta_k = \varepsilon_k - J_H - \mu$ and $\Gamma = 0$ at the ground state with full polarization $M = 1$. The minority band has different nature. We see the quasiparticle residue $z(M) \rightarrow 0$ and the dispersion $\zeta_k = \text{const.}$ as $M \rightarrow 1$. This is well understood from Anderson-Hasegawa picture, that strong J_H projects out the low energy minority band and also prohibits hopping among sites. What is found here that is not available through a simple mean-field treatment of the Anderson-Hasegawa's model is the lifetime of the minority electrons. The minority band has large linewidth $\sim W$ due to large amount of scattering with localized spins in opposite direction, so that the propagation of minority electrons are incoherent and diffusive. Then we have the width of the minority band $\sim W$ despite real part of the quasi-particle energy becomes dispersionless.

2. Stoner spectrum

Stoner susceptibility is calculated by

$$\chi(q, z) = \frac{1}{\beta N} \sum G(k + q, i\omega_n + z)G(k, i\omega_n). \quad (2.6)$$

Here, correlation effects are taken into account through the self-energy correction in G . In Fig. 2 we show $\text{Im}\chi(Q, \omega)$ at the Brillouin zone corner $Q = (\pi, 0, 0)$ for various temperatures, at $J_H/W = 2$ and $x = 0.3$. We see two-peak structure at $\omega \sim 0$ and $\omega \sim 2J_H$ which is explained from the J_H -split DOS. The Stoner absorption is produced from a particle-hole pair excitations with spin flip, which produces a peak at low energy from intra-band processes and another peak at $\omega \sim 2J_H$ from interband processes.

Let us investigate the low energy part more precisely. We see that at small ω we have ω -linear relation, *i.e.* $\text{Im}\chi \propto \omega$ at $\omega \ll W$. Coefficients for ω -linear part decrease by decreasing the temperature. In Fig. 3 we show the coefficient for ω -linear part $D'' = \partial \text{Im}\chi(Q, \omega)/\partial \omega|_{\omega \rightarrow 0}$ as a function of normalized magnetization M^* at wave vector Q . As a result we find

$$\text{Im}\chi(Q, \omega) \propto (1 - M^{*2})\omega \quad (2.7)$$

for small values of ω . The relation (2.7) is observed at all values of q with weak q dependence.

This is explained from the fact that the low energy Stoner absorption is constructed from a process with combinations of a minority particle and a majority hole carriers. Since the majority and the minority bands have the spectral weight proportional to $(1 + M)/2$ and $(1 - M)/2$, respectively, the low energy part of the Stoner absorption is proportional to $1 - M^2$. The ω -linear behavior comes from the Fermi distribution function as is the case for the noninteracting Fermion, since the initial and final state is limited in energy $|\epsilon - \mu| < \omega$. In our case, the incoherence of the minority band gives the weak q dependence. Thus we have the scaling relation $\text{Im}\chi \propto (1 - M^{*2})\omega q$. The weak q dependence is in large contrast with the conventional weak ferromagnet where minority band is also coherent, which gives strong q dependence through its band structure.

3. Optical spectrum

Within the framework of the dynamical mean-field theory, optical conductivity at finite frequencies is obtained through the Kubo formula as

$$\sigma(\omega) = \sigma_0 \sum_\sigma \int d\omega' I_\sigma(\omega', \omega' + \omega) \frac{f(\omega') - f(\omega' + \omega)}{\omega}, \quad (2.8)$$

where

$$I_\sigma(\omega_1, \omega_2) = \int N_0(\epsilon) d\epsilon W^2 A_\sigma(\epsilon, \omega_1) A_\sigma(\epsilon, \omega_2). \quad (2.9)$$

Here, the spectral weight function A is defined by

$$A_\sigma(\epsilon, \omega) = -\frac{1}{\pi} \text{Im}G_\sigma(\epsilon, \omega + i\eta), \quad (2.10)$$

while f is the Fermi distribution function. The constant σ_0 gives the unit of conductivity.

We see (i) the two-peak structure of $\sigma(\omega)$ at $\omega \sim 0$ and $\omega \sim 2J_H$, and (ii) the transfer of spectral weight by temperature. The two-peak structure is due to the splitting of the DOS at $\pm J_H$. The peak at $\omega \sim 0$ corresponds to the Drude peak which is due to the particle-hole excitation in the lower subband, while $\omega \sim 2J_H$ part is due to the interband process between J_H -split bands. At $T > T_c$, where DOS is equally split for up and down spins, the two-peak structure is most pronounced. In the ferromagnetic phase, the weight is shifted from the high energy peak to the low energy peak, corresponding to the DOS structure controlled by the magnetism. The width of $\sigma(\omega)$ for Drude part becomes narrower as temperature becomes lower, due to the reduction of the imaginary part of the self-energy for the majority channel. The width of the interband process at $\omega \sim 2J_H$ is kept as large as a fraction of W , since this process is transition into the minority channel which has the incoherent nature with linewidth $\sim W$.

In §4, we will show the results for $\sigma(\omega)$ in more detail, in comparison with experimental data, including the scaling relation for the transfer of spectral weight as well as the fitting.

III. SPIN EXCITATION AND STONER ABSORPTION

A. Experimental

Single crystals of $(\text{La}_{1-x-y}\text{Y}_y)\text{Sr}_x\text{MnO}_3$ (typically $6\phi \times 80$ mm) were grown by the floating-zone method. The end part (30–40 mm) were used for neutron measurements. In order to study the effects of electronic bandwidth, three samples were chosen; $y = 0.00, 0.05$ and 0.10 with the Sr concentration fixed at $x = 0.20$. The tolerance factor t , which is defined as $t = (r_A + r_O)/\sqrt{2}(r_B + r_O)$ for ABO_3 perovskites and scales with the band width, decreases with doping Y; 0.908, 0.906 and 0.903 for $y = 0.00, 0.05$ and 0.10 , respectively. These values are, however, still closer to unity than $\text{La}_{0.8}\text{Ca}_{0.2}\text{MnO}_3$ (0.894) and $\text{Pr}_{0.8}\text{Ca}_{0.2}\text{MnO}_3$ (0.877). Neutron-scattering measurements were carried out using the triple-axis spectrometer TOPAN at the JRR-3M reactor in Japan Atomic Energy Research Institute. Typical condition employed was the fixed final energy at 14.7 meV with horizontal collimation of Blank-30'-Sample-60'-Blank. The (002) reflection of pyrolytic graphite (PG) is used to monochromatize and analyze neutrons. A PG filter was used to reduce higher-order contaminations in the incident beam. The Curie temperature T_C and its Gaussian distribution ΔT_C was determined using the temperature dependence of the (100)_{Cubic} peak intensity; T_C (ΔT_C) is 306(1.1), 281(1.4) and 271(10) K for $y = 0.00, 0.05$ and 0.10 , respectively.

The spin-wave dispersion curves for studied $(\text{La}_{1-x-y}\text{Y}_y)\text{Sr}_x\text{MnO}_3$ samples show an isotropic behavior in the measured (q, ω) range, $q < 0.40 \text{ \AA}^{-1}$ and $\hbar\omega < 20$ meV, and follow well with $\hbar\omega(q) = Dq^2 + E_0$, typical of ferromagnetic spin-wave dispersion in low q and low ω range. In order to study the temperature dependence of spin-wave stiffness D , we have performed constant- Q scans at (1.1 1.1 0) where well-defined peak profiles are obtained in a wide temperature range. Each peak profile was fitted with the spin-wave scattering cross section including the finite life-time \hbar/Γ_q convoluted with a proper instrumental resolution. Figure 4 shows thus obtained temperature dependence of D . Error bars indicate fitting errors. Dashed lines are guides to the eye. Softening of spin wave dispersion $\omega(q, T)$ is observed as temperature approaches T_c .

B. Scaling relation

Spin wave dispersion relation throughout the Brillouine zone as well as the temperature dependence of the magnon linewidth is first reported by Perring *et al.* for $\text{La}_{0.7}\text{Pb}_{0.3}\text{MnO}_3$.¹⁹ The cosine-band like dispersion as well as its slight softening at the zone boundary is reproduced by the spin wave expansion of the double-exchange model,²⁰ and a qualitative explanation for the linewidth is through the Stoner absorption mechanism is also discussed there. In this paper, we describe the temperature dependence of the linewidth more precisely through a scaling relation between the magnetization and the magnon linewidth.

Within the linear spin wave theory of the double-exchange model at $J_H \gg W$,²⁰ the dispersion relation ω_q as well as its linewidth Γ_q is obtained by

$$\omega_q = \text{Re} \Pi(q, \omega_q), \quad (3.1)$$

$$\Gamma_q = \text{Im} \Pi(q, \omega_q), \quad (3.2)$$

where the magnon self-energy Π is calculated by

$$\Pi(q, \omega) = (J_H^2/St)\chi(q, \omega), \quad (3.3)$$

and $\chi(q, \omega)$ is the Stoner susceptibility. Note that in the large Hund's coupling region the magnon bandwidth J_{magnon} is scaled by W as is the case for T_c . Namely, in the region $J_H/W \gg 1$ the leading order of J_{magnon}/W is $1/S$ and does not contain J_H due to the nature of Hund's coupling as a projection. Indeed, the result is identical in the limit $J_H \rightarrow \infty$ treated by Kubo and Ohata.²¹ This justifies the linear spin wave theory at large J_H region, at least asymptotically in the large $1/S$ limit.

Higher order terms in the asymptotic $1/S$ expansion give vertex corrections. However, vertex corrections may be neglected by restricting ourselves in the low temperature region where magnon density is low, and in the sufficiently large doping concentration region where electron kinetic energy is larger than the magnon energy. Accuracy of the linear spin wave calculation in the sufficiently

doped region is shown by comparison with $S = 1/2$ model,²² which at the same time shows the softening of the zone boundary magnon dispersion when electron kinetic energy is small at low electron/hole doping.

Let us now assume that the major origin of the linewidth broadening is due to Stoner absorption mechanism, which implies that we neglect magnon-magnon interactions as well as other mechanisms of extrinsic origins. From eq. (2.7) we obtain

$$\Gamma_q = \alpha_q(1 - M^{*2})\omega_q \quad (3.4)$$

where α_q is a dimensionless function of q . In other words, the definition of the spin stiffness is extended into a complex number $D = D' + iD''$ and the dispersion as well as its linewidth at small q region is expressed as $\omega_q = D'q^2$ and $\Gamma_q = D''q^2$.

As for the experiment, we show the inverse lifetime $\Gamma(q, T)$ versus $(1 - M^{*2})\omega(q, T)$ at the inset of Fig. 4. From the figure we see that inverse lifetime is fitted in the form

$$\Gamma(q, T) = \Gamma_0(q) + \alpha_q(1 - M^{*2})\omega(q, T). \quad (3.5)$$

Temperature dependence is scaled in a way consistent with theoretical result for DE systems. Γ_0 is the T -independent part of the spin wave lifetime, *i.e.* $\Gamma(q, T \rightarrow 0) = \Gamma_0(q)$, which increases systematically by increasing the ratio of Y atoms.

From the data we consider that the temperature dependent part of the magnon damping mechanism is mainly due to Stoner absorption which does not show large change by Y doping. Large change by Y doping is seen in the temperature independent part Γ_0 . We speculate that the origin of Γ_0 is mainly extrinsic effects such as disorder and inhomogeneity of the sample. Substitution of La by Y creates the decrease of $\langle r_A \rangle$ which causes a reduction of the average electron hopping, as well as the local Mn-O-Mn bond distortion. In both cases, they contribute to a charge inhomogeneity through charge segregation²³⁻²⁵ or localization. Since spin stiffness is a function of charge concentration, especially $D \propto x$ in the region of interest here,²⁶ charge inhomogeneity creates distribution of spin stiffness in a mesoscopic scale. Inhomogeneities in magnetism as well as charge distributions are also reported in (La,Ca)MnO₃ by various measurements including μ SR,²⁷ Raman²⁸ and photoemission.²⁹ Broadening of the spin wave linewidth at the zone boundary observed at lower T_c compounds³⁰ might also indicate the inhomogeneities in mesoscopic length scale.

IV. CHARGE EXCITATION BETWEEN THE J_H -SPLIT BANDS

A. Experimental

Thin films of $R_{0.6}\text{Sr}_{0.4}\text{MnO}_3$ ($R=\text{La}$, $\text{La}_{0.5}\text{Nd}_{0.5}$, $\text{Nd}_{0.5}\text{Sm}_{0.5}$ and $\text{Nd}_{0.25}\text{Sm}_{0.75}$) with thickness of ~ 100 nm

were fabricated using a vacuum pulsed laser deposition (PLD) apparatus. Details of film synthesis are described in Ref. 15. The compound was deposited on to a MgO (100) substrate, since the substrate is transparent in a wide energy region of 0.1 - 5.0 eV and is suitable for the absorption measurements. An absorption coefficient α was determined from transmission spectra using the standard formula neglecting a multi-reflection effect, since the optical density of our films is larger than 0.7 in the spectral region investigated. X-ray diffraction measurements revealed that the obtained films were (110)-oriented in the pseudo-cubic setting. Thicknesses of the films were measured by a scanning electron microscope (SEM).

Temperature dependence of magnetization M was measured under a field of 0.5 T after cooling down to 5 K in zero field (ZFC), using a superconducting quantum interference device (SQUID) magnetometer. T_C was determined from the inflection point of the $M-T$ curve. With decreasing r_A , T_C decreases from ≈ 325 K for $R=\text{La}$, ≈ 315 K for $\text{Nd}_{0.5}\text{Sr}_{0.5}$, ≈ 175 K for $\text{Nd}_{0.5}\text{Sm}_{0.5}$ to ≈ 90 K for $\text{Nd}_{0.25}\text{Sm}_{0.75}$. The suppression of T_C is originated in reduction of the Mn-O-Mn bond angle, and hence the transfer integral t (*chemical pressure* effect^{31,32}). In other words, we can control the W -value with changing the averaged ionic radius r_R of the trivalent rare-earth atom R^{3+} .

B. Temperature-dependent absorption spectra

Figure 5 shows variation of the absorption spectrum $\alpha(\omega)$ ($= (4\pi/cn(\omega)) \cdot \sigma(\omega)$) in the temperature range of 6 - 400 K for $\text{La}_{0.6}\text{Sr}_{0.4}\text{MnO}_3$ with maximal- W ($T_C \approx 325$ K). Here, refractive index $n(\omega)$ is almost constant, and hence $\alpha(\omega) \propto \sigma(\omega)$, above ~ 0.5 eV. With decreasing temperature, a large transfer of spectral weight from ~ 3 eV to ~ 0 eV is observed. This has been interpreted as the spectral weight transfer from the interband transition between the J_H -split bands (J_H -gap excitation) to the intraband transition within the lower band¹⁵. To analyze the spectral behavior more in detail, we extract the temperature dependent component $\alpha_T(\omega)$:

$$\alpha_T(\omega) = \alpha(\omega) - \alpha_{CT}(\omega). \quad (4.1)$$

The temperature-independent component $\alpha_{CT}(\omega)$ (hatched region in Fig.5) is ascribed to the charge-transfer (CT) type transitions from ligand p states to Mn $3d$ levels¹⁵. Figure 6(a) shows the $\alpha_T(\omega)$ spectra for $\text{La}_{0.6}\text{Sr}_{0.4}\text{MnO}_3$. The absorption band located at ~ 3 eV, which corresponds to the J_H -gap excitation, significantly decreases in intensity with decreasing temperature. This is because the density of state (DOS) of the up- (down-) spin states in the upper (lower) J_H -split band decreases with t_{2g} -spin polarization. The lost spectral weight is transferred into the lower-lying Drude component (≤ 1 eV). Similar behaviors are observed in the spectra for the small- W compounds, *e.g.*, $R=\text{Nd}_{0.5}\text{Sm}_{0.5}$

and $\text{Nd}_{0.25}\text{Sm}_{0.75}$, though a small polaron band becomes discernible at ~ 1.5 eV.³³

The temperature-dependent behavior of the J_{H} -gap excitation is well reproduced by the double-exchange model that include only J_{H} - and t -terms. Figure 6(b) represents the calculated optical conductivity $\sigma(\omega)$ with $n=\infty$ and $S=\infty$ approximation. The two parameters, i.e., $W(=1$ eV) and $J_{\text{H}}(=1.5$ eV), are estimated from the J_{H} -gap band in Fig.6(b). As seen in Fig.6, the calculated results well reproduce not only the overall profile but also the temperature dependence of the J_{H} -gap band around ~ 3 eV. Note that the estimate for T_{C} in the present model ($=292$ K) is very close to the experimentally derived value ($=325$ K).

In the low energy Drude region (≤ 1.5 eV), however, the temperature-dependent behavior of $\alpha_{\text{T}}(\omega)$ (Fig.6(a)) is qualitative different from the calculation (Fig.6(b)). The Drude component monotonously increases with decreasing temperature, but does not show any sharpening behavior like the calculation. The discrepancy suggests that additional factors, such as dynamical Jahn-Teller effect^{34,35} or degeneracy of the e_g -orbitals^{36,37}, might be necessary to reproduce the low energy charge excitation.

C. Scaling relation

In doped manganites, DOS of the e_g -electrons is governed by confirmation of the local t_{2g} -spin due to the strong on-site charge interaction J_{H} . Therefore, the apparent temperature dependence of $\alpha_{\text{T}}(\omega)$ spectrum (Fig.6(a)) should be ascribed to the induced magnetization M^* . In Fig.7(a), we plot the spectral weight of the J_{H} -gap band,

$$S_{J_{\text{H}}} \equiv \int_{2.2\text{eV}}^{4.0\text{eV}} \alpha_{\text{T}}(\omega) d\omega, \quad (4.2)$$

for $R_{0.6}\text{Sr}_{0.4}\text{MnO}_3$ as a function of $1 - M^*$. The values of $M^* = M(T)/M(0)$ were estimated under a field of 0.5 T to avoid the complexity arising from the nonremanent behavior of the present system. Change of the $S_{J_{\text{H}}}$ -value with temperature scales well with $1 - M^*$. As shown in the Fig.7(b), above scaling relation is reproduced by calculation based on the double exchange model,

$$S_{\text{theory}} = \int_{\omega \sim 2J_{\text{H}}} \sigma(\omega) d\omega, \quad (4.3)$$

where integration is performed at the high energy peak region around $\omega \sim 2J_{\text{H}}$.

These scaling relation (4.4) and (4.3) are explained as follows. For the charge excitations, interband optical absorption is constructed by spin conserving process of scattering lower band electrons into upper bands. The initial and final state weight is again $(1 + M^*)/2$ and $(1 - M^*)/2$, respectively, and the optical absorption is proportional to $(1 - M^{*2})$. Phenomenologically, this is

because the DOS of the up- (down-) spin states in the lower (upper) J_{H} -split band increases as $\propto (1 + M^*)$, while the up- (down-) spin states in the upper (lower) band decreases as $\propto (1 - M^*)$.

Finally, let us comment on the strength of the J_{H} -gap band. The spectral weight $S_{J_{\text{H}}}$ is expressed as:

$$S_{J_{\text{H}}} = (2\pi^2 e^2 N_0 / cm_0 \bar{n}) \cdot f_0 \cdot (1 - M^{*2}), \quad (4.4)$$

where averaged refractive index \bar{n} is ≈ 2 around the J_{H} -gap transition. f_0 is the oscillator strength for the $d-d$ transition per one e_g -electron. As seen in Fig. 7, the magnitude of $S_{J_{\text{H}}}$ at $M^* \approx 0$ (high temperature limit) is strongly material dependent, indicating that the f_0 -value increases from ≈ 0.04 for $R=\text{Nd}_{0.5}\text{Sm}_{0.5}$ to ≈ 0.08 for La. Remember that f_0 is proportional to square of the transition matrix element between the neighboring e_g -orbitals, which is nearly proportional to t , and hence W . Recently, Machida *et al.*³³ have evaluated the W -values for $R_{0.6}\text{Sr}_{0.4}\text{MnO}_3$ from $\alpha(\omega)$ spectra: W increases from ≈ 0.6 eV for $R=\text{Nd}_{0.5}\text{Sm}_{0.5}$ to ≈ 0.8 eV for $R=\text{La}$. Such a material-dependent W qualitatively explain the observed enhancement of the f_0 -value.

V. DISCUSSION

The general role of the DE mechanism to the electronic structure is understood through the half-metallic DOS at the ground state and the shift of the spectral weight by the magnetic fluctuations. As a consequence of the DOS structure, spin and charge dynamics are influenced through a particle-hole channel. In experiments, optical conductivity $\sigma(\omega)$ and spin wave linewidth Γ_q show scaling relations in agreement with the theory.

Let us discuss the two different energy scale of the DE system and CMR materials which arises from DOS structure controlled by magnetism. The electronic structure changes its spectrum by magnetization in the scale of $2J_{\text{H}} \sim 3\text{eV}$ if both of the J_{H} -split band are concerned. The scale of the change in the spectrum for a case when only the lower sub-band is playing a role is $W \sim 1\text{eV}$. However, the energy scale concerning the magnetic properties has a smaller energy scale determined by the DE interaction, $J_{\text{DE}} \sim T_{\text{c}} \sim 10^{-2}\text{eV}$. Thus a small change in magnetization causes a large change in electronic structures, *e.g.* a change of temperature in the scale of 300K causes the change in optical spectrum at 3eV. Such a huge change in DOS spectrum controlled by a small amount of magnetic field is considered to cause sensitive change of transport properties as well as other thermodynamical properties.³⁸

Similar phenomena happens for a correlated electron system in the vicinity of the Mott transition.³⁹ This case, the coherent temperature becomes small compared to the bandwidth, $T_{\text{coh}} \ll W$, so that the change in the scale of T_{coh} produce a large change in the electronic structures. For the DE systems, however, the small energy

scale J_{DE} and the large energy scale W as well as J_H coexists robustly, and such phenomena is commonly observed throughout the doping concentration.

In order to compare the theory with CMR compounds, we need to consider that their behavior changes by A-site substitutions. Let us concentrate to the region $x \sim 1/3$ where it is far from antiferromagnetic insulating phase at $x \sim 0$ and the region with charge and orbital ordering at $x \sim 0.5$. The nature of the compound is roughly classified by the average radius of the A-site ions $\langle r_A \rangle$.^{31,32,40} Compounds with larger $\langle r_A \rangle$ have to larger tolerance factor and larger Mn-O-Mn bond angle, which in general increase the effective electron hopping and hence T_c . However, we should note that it is still controversial whether the phase diagram is controlled mostly by the bandwidth alone, *e.g.* ionic size variation $\sigma(r_A)$ also plays some role to change T_c ,⁴¹ and also the decrease of T_c at lower T_c region is much larger compared to the estimate from the change in $\langle r_A \rangle$.

A canonical example for the high T_c compounds is (La,Sr)MnO₃ which is resistivity wise a good metal below T_c , and incoherent metal with $\rho(T)$ near Mott's limit. The most well investigated compound (La,Ca)MnO₃, where Ca substitution creates smaller $\langle r_A \rangle$ and larger $\sigma(r_A)$, has lower T_c , and shows metal to insulator transition at around T_c . Compounds with smaller $\langle r_A \rangle$ such as (Pr,Ca)MnO₃ do not undergo ferromagnetic transition and stay insulating.³

As long as the wide-banded compound with high doping are concerned, *e.g.* (La,Sr)MnO₃ at $x = 0.2 \sim 0.4$, the DE Hamiltonian accounts for several experimental data concerning the ferromagnetism and the transport. Curie temperature is estimated by various methods^{11,23,42} and is consistent with experiments in magnitude as well as the doping dependence. The resistivity is calculated by the dynamical mean-field approach^{10,13} and the result is consistent with the experimental data for resistivity^{43,44} which show metallic behavior $d\rho/dT > 0$ at $T > T_c$ as well as the absolute value $\rho(T) = 2 \sim 4\text{m}\Omega\text{cm}$ which is not so large compared to the Mott limit. Universal behavior of the magnetoresistance in the form $-\Delta\rho/\rho_0 \propto M^{*2}$ is also consistent between theory and experiment.

Together with the scaling relations described in this paper, DE Hamiltonian alone explains various experimental data in manganites with high T_c . The mechanism of MR in the single-crystal of these high T_c compounds are understood from double-exchange alone, namely due to spin disorder scattering.^{10,21,45-47} It is noteworthy that the local Jahn-Teller distortion is reported even in the metallic phase of (La,Sr)MnO₃,⁴⁸ which might indicate that the effect of the lattice distortion (small polaron formation) is not so prominent for these compounds.

It has been discussed that the roles of other interactions such as lattice distortion⁴⁹ or orbital fluctuation⁵⁰ are important in (La,Sr)MnO₃. Especially, the discrepancies in Curie temperature as well as resistivity between the double-exchange alone model and CMR manganites

are emphasized. However, as discussed above, accurate treatment on theoretical calculation and the bulk measurement of single crystal samples without grain effects show that the double-exchange model explains various thermodynamical properties of the high T_c compounds such as (La,Sr)MnO₃.

Let us now discuss the properties of compounds with lower T_c , *e.g.* (La,Ca)MnO₃, which qualitatively show different behaviors. One of the major difference is that the resistivity above T_c shows semiconductive temperature dependence. Several theories based on microscopic models are proposed. Polaron effects of Jahn-Teller distortions are introduced to explain the metal-insulator transition from the point of view of large polaron to small polaron crossover by magnetism.^{34,51} The idea of Anderson localization due to spin disorder as well as diagonal charge disorder has also been discussed.^{47,52-56}

Many of these proposals relate magnetism and transport through the change of the hopping matrix element $t_{\text{eff}}(T, H)$ as discussed by Anderson and Hasegawa.² Namely, in general, these scenarios discuss the existence of the critical value of hopping t_c determined by polaron size or mobility edge, and explain the metallic state as large hopping region $t_{\text{eff}}(T, H) > t_c$ and the insulating state as small hopping region $t_{\text{eff}}(T, H) < t_c$. However, in order to explain the experiments for resistivity, these scenario requires fine tuning of the parameters in the following sense; to explain the fact that the metal-insulator transition always occurs in the vicinity of T_c for various A-site substitution in both ionic radius and average valence changes, they require the pinning of the critical hopping $t_c \sim t_{\text{eff}}(T = T_c)$ for any values of carrier concentration as well as bandwidth and A-site randomness. Note that t_{eff} is determined by the short range spin correlation $\langle S_i \cdot S_j \rangle$ and is a smooth and continuous function of temperature without an anomaly at T_c . It is also required to explain the absence of the metal-insulator transition in high- T_c compounds such as (La,Sr)MnO₃ at $x \sim 1/3$.

In order to investigate such controversial issues, it is important to discuss the difference of the resistivity properties in these compounds in comparison with other properties from the point of view of deviation from DE behavior. Concerning the charge dynamics, the effect of the A-site substitution is investigated as follows. Optical conductivity measurements^{32,57,58} show that the J_H -split peak at around 3eV investigated in this paper remains as bandwidth is changed from wide to narrow. The bandwidth control causes changes in the spectrum at the peak structure around $\sim 1\text{eV}$ and the infrared quasi-Drude (incoherent) structures. In a narrow band system, Machida *et al.*^{33,59} has found a characteristic absorption band at $\sim 1.5\text{eV}$ originated in transition of small polarons. The small polaron band disappear in the ferromagnetic metallic state.

For the spin dynamics, spin wave dispersion as well as its linewidth has been investigated. For wide-bandwidth compounds, spin wave dispersion¹⁹ in La_{0.7}Pb_{0.3}MnO₃

which roughly shows a cosine-band type dispersion is explained by the DE Hamiltonian.^{20,22,60} For (La,Sr)MnO₃, the residual linewidth $\Gamma_0(q)$ behaves as $\sim q^4$ in the insulating region at $x \sim 0.15$,⁶¹ which is understood as magnon-magnon scattering effect, and as $\sim q^2$ in the metallic region at $x \sim 0.2$,⁶² which is speculated to be due to inhomogeneity effect through spin stiffness distribution. For lower T_c compounds, there exists a systematic behavior that broadening of the spin wave dispersion is prominent at the zone boundary.³⁰ Another unconventional feature in these compounds is the presence of the central peak well below T_c ,⁶³ which indicates the presence of the magnetic cluster and its diffusive dynamics. From the spin diffusion constant, the correlation length of the spin clusters are estimated to be $\xi \sim 10\text{\AA}$. Neutron elastic scattering measurements also observed the ferromagnetic cluster with correlation length $\xi \sim 20\text{\AA}$.^{64,65}

Thus from the points of view of charge and spin dynamics, the observed systematic change as T_c become lower is considered to be the formation of magnetic cluster with typical length scale of $\xi < 10^2\text{\AA}$, accompanied by lattice distortion, or magnetoelastic polaron. Inhomogeneities in charge and magnetic structures²⁷⁻²⁹ suggest that such polaronic cluster remain even at low temperatures. Possible micrograin formation due to charge segregation as well as phase separation between ferromagnetic and antiferromagnetic domains has also been discussed.⁶⁶⁻⁶⁸

In the presence of ferromagnetic clusters, or magnetically isolated half metallic nanodomains, one can discuss the tunneling MR mechanism for half metals as the origin of the CMR behavior, as is commonly the case for polycrystals.⁶ Instability of electronic phase separation²³ is a candidate for the initial driving force for such phenomena, which is stabilized to form droplet structures due to long range Coulomb interactions. Another possibility is the effect of static potential disorder due to A-site cation R^{3+} - A^{2+} distributions which causes charge inhomogeneities, as well as self-trapping effect of lattice polarons. The idea is consistent with the phenomenological explanation of resistivity in (La,Ca)MnO₃ by the Two-fluid model⁶⁹ which discusses the coexistence of a metallic conductivity path and an activation-type polaronic conductivity.

To summarize, we investigated spin and charge excitation of DE by both theoretical and experimental approaches. We see the scaling behavior in spin wave lifetime as well as interband optical spectrum. These features are well understood by the magnetization dependence of the DOS with half-metallic behaviors. Origin of the magnetoresistance is discussed as a spin-disorder scattering in the wide bandwidth region and tunneling MR due to half-metallic behavior in the narrow bandwidth region.

ACKNOWLEDGMENTS

N.F. is supported by the Mombusho Grant for overseas research. N.F. thanks E. Dagotto, A. Moreo and C.M. Varma for fruitful discussions. Y.M would like to thank A. Machida for his help in optical measurements. The work was supported by a Grant-In-Aid from Precursory Research for Embryonic Science and Technology (PRESTO), Japan Science and Technology Cooperation (JST), Japan.

-
- ¹ C. Zener, Phys. Rev. **82**, 403 (1951).
 - ² P. W. Anderson and H. Hasegawa, Phys. Rev. **100**, 675 (1955).
 - ³ For reviews on recent experiments, see A. P. Ramirez, J. Phys. **CM9**, 8171 (1997), and references therein.
 - ⁴ For reviews on recent theoretical works, see A. R. Bishop and H. Röder, cond-mat/9703148, and references therein.
 - ⁵ For a review on half metals, see D. Khomskii and G. Sawatzky, Solid State Comm. **102**, 87 (1997).
 - ⁶ H. Hwang, S.-W. Cheong, N. Ong, and B. Batlogg, Phys. Rev. Lett. **77**, 2041 (1996).
 - ⁷ J. Sun *et al.*, Appl. Phys. Lett. **69**, 3266 (1996).
 - ⁸ K. Steenbeck *et al.*, Appl. Phys. Lett. **71**, 968 (1997).
 - ⁹ N. D. Mathur *et al.*, Nature **387**, 266 (1997).
 - ¹⁰ N. Furukawa, J. Phys. Soc. Jpn. **63**, 3214 (1994).
 - ¹¹ N. Furukawa, J. Phys. Soc. Jpn. **64**, 2754 (1995).
 - ¹² N. Furukawa, J. Phys. Soc. Jpn. **64**, 2734 (1995).
 - ¹³ N. Furukawa, J. Phys. Soc. Jpn. **64**, 3164 (1995).
 - ¹⁴ N. Furukawa and K. Hirota, Physica B **241-243**, 780 (1998).
 - ¹⁵ Y. Moritomo *et al.*, Phys. Rev. **B56**, 5088 (1997).
 - ¹⁶ A. Georges, G. Kotliar, W. Krauth, and M. J. Rozenberg, Rev. Mod. Phys. **68**, 13 (1996).
 - ¹⁷ Th. Pruschke, M. Jarrell, and J. Freericks, Adv. in Phys. **44**, 187 (1995).
 - ¹⁸ J.-H. Park *et al.*, Nature **392**, 794 (1998).
 - ¹⁹ T. G. Perring *et al.*, Phys. Rev. Lett. **77**, 711 (1996).
 - ²⁰ N. Furukawa, J. Phys. Soc. Jpn. **65**, 1174 (1996).
 - ²¹ K. Kubo and N. Ohata, J. Phys. Soc. Jpn. **33**, 21 (1972).
 - ²² T. A. Kaplan and S. D. Mahanti, J. Phys. Cond. Mat. **9**, L291 (1997).
 - ²³ S. Yunoki *et al.*, Phys. Rev. Lett. **80**, 845 (1998).
 - ²⁴ M. Kagan, D. Khomskii, and M. V. Mostovoy, cond-mat / 9804213 (unpublished).
 - ²⁵ Phase separation in the weak exchange limit ($J_H \ll W$) is also discussed in E. L. Nagaev, Physica B **230-232**, 816 (1997). Note that the ground state is not half metal in this regime.
 - ²⁶ K. Hirota, N. Kaneko, A. Nishizawa, and Y. Endoh, J. Phys. Soc. Jpn. **65**, 3736 (1996).
 - ²⁷ R. H. Heffner *et al.*, Phys. Rev. Lett. **77**, 1869 (1996).
 - ²⁸ S. Yoon *et al.*, Phys. Rev. **B58**, 2795 (1998).
 - ²⁹ C. H. Booth *et al.*, Phys. Rev. **B57**, 10440 (1998).

- ³⁰ H. Hwang *et al.*, Phys. Rev. Lett. **80**, 1316 (1998).
³¹ H. Hwang *et al.*, Phys. Rev. Lett. **75**, 914 (1995).
³² Y. Moritomo, H. Kuwahara, and Y. Tokura, J. Phys. Soc. Jpn. **66**, 556 (1997).
³³ A. Machida, Y. Moritomo, and A. Nakamura, Phys. Rev. B, in press (unpublished).
³⁴ A. J. Millis, B. I. Shraiman, and R. Mueller, Phys. Rev. Lett. **77**, 175 (1996).
³⁵ A. J. Millis, R. Mueller, and B. I. Shraiman, Phys. Rev. **B54**, 5405 (1996).
³⁶ H. Shiba, R. Shiina, and A. Takahashi, J. Phys. Soc. Jpn. **66**, 941 (1997).
³⁷ P. de Brito and H. Shiba, Phys. Rev. **B57**, 1539 (1998).
³⁸ A. Asamitsu *et al.*, Nature **373**, 407 (1995).
³⁹ M. J. Rozenberg *et al.*, Phys. Rev. Lett. **75**, 105 (1995).
⁴⁰ P. Radaelli *et al.*, Phys. Rev. **B56**, 8265 (1997).
⁴¹ L. M. Rodriguez-Martinez and J. P. Attfield, Phys. Rev. **B54**, 15622 (1996).
⁴² H. Röder, R. Singh, and J. Zang, Phys. Rev. **B56**, 5084 (1997).
⁴³ Y. Tokura *et al.*, J. Phys. Soc. Jpn. **63**, 3931 (1994).
⁴⁴ A. Urushibara *et al.*, Phys. Rev. **B51**, 14103 (1995).
⁴⁵ T. Kasuya, Prog. Theo. Phys. **16**, 58 (1956).
⁴⁶ M. E. Fisher and J. Langer, Phys. Rev. Lett. **20**, 665 (1968).
⁴⁷ E. L. Nagaev, Phys. Rev. **B58**, 816 (1998).
⁴⁸ D. Louca *et al.*, Phys. Rev. **B56**, 8475 (1997).
⁴⁹ A. J. Millis, P. B. Littlewood, and B. I. Shraiman, Phys. Rev. Lett. **74**, 5144 (1995).
⁵⁰ S. Ishihara, J. Inoue, and S. Maekawa, Physica C **263**, 130 (1996).
⁵¹ H. Röder, J. Zang, and A. R. Bishop, Phys. Rev. Lett. **76**, 1356 (1996).
⁵² C. M. Varma, Phys. Rev. **B54**, 7328 (1996).
⁵³ E. Müller-Hartmann and E. Dagotto, Phys. Rev. **B54**, 6819 (1996).
⁵⁴ R. Allub and B. Alascio, Sol. State Comm. **99**, 613 (1996).
⁵⁵ Q. Li, J. Zang, A. R. Bishop, and C. Soukoulis, Phys. Rev. **B56**, 4541 (1997).
⁵⁶ L. Sheng, D. Xing, D. Sheng, and C. Ting, Phys. Rev. **B56**, 7053 (1997).
⁵⁷ J. H. Jung *et al.*, Phys. Rev. **B57**, 11043 (1998).
⁵⁸ M. Quijada *et al.*, cond-mat/9803201 (unpublished).
⁵⁹ A. Machida, Y. Moritomo, and A. Nakamura, submitted to PRB (unpublished).
⁶⁰ X. Wang, Phys. Rev. **B57**, 7427 (1998).
⁶¹ L. Vasiliu-Doloc *et al.*, J. Appl. Phys. **81**, 5491 (1997).
⁶² A. Moudden, L. Vasiliu-Doloc, L. Pinsard, and A. Revcolevschi, Physica B **241-243**, 276 (1998).
⁶³ J. Lynn *et al.*, Phys. Rev. Lett. **76**, 4046 (1996).
⁶⁴ J. D. Teresa *et al.*, Phys. Rev. **B54**, 12689 (1996).
⁶⁵ J. Fernandez-Baca *et al.*, Phys. Rev. Lett. **80**, 4012 (1998).
⁶⁶ G. Allodi *et al.*, Phys. Rev. **B56**, 6036 (1997).
⁶⁷ T. Perring, G. Aeppli, Y. Moritomo, and Y. Tokura, Phys. Rev. Lett. **78**, 3197 (1997).
⁶⁸ M. Hennion *et al.*, cond-mat/9806272 (unpublished).
⁶⁹ M. Jaime and M. Salamon (unpublished).

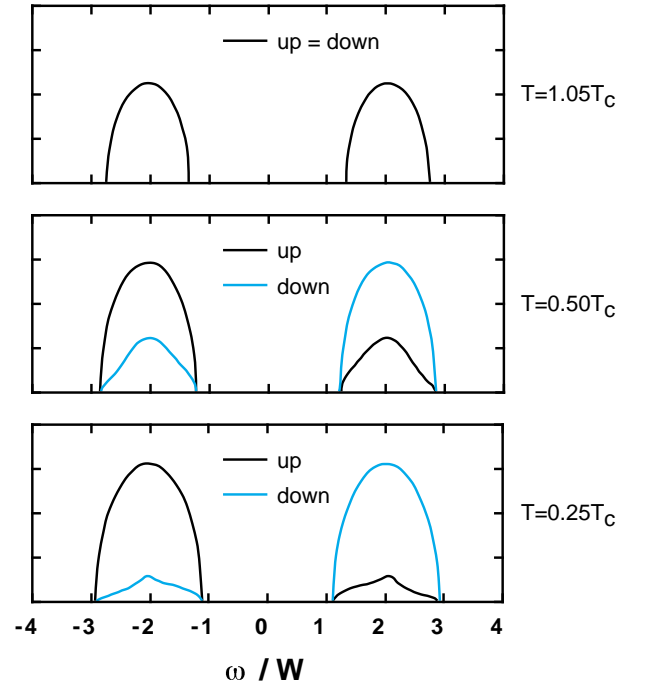


FIG. 1. Electron DOS by DMF calculation at $J_H/W = 2$ and $x = 0.2$.

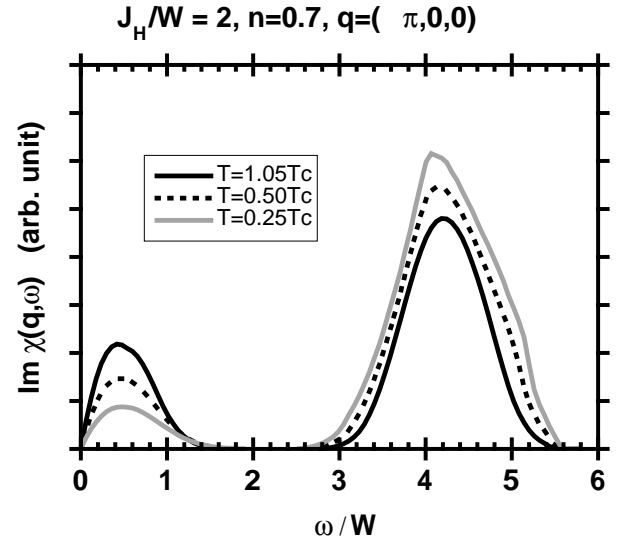


FIG. 2. Stoner absorption $\text{Im}\chi(q, \omega)$ at $q = (\pi, 0, 0)$ for various temperatures.

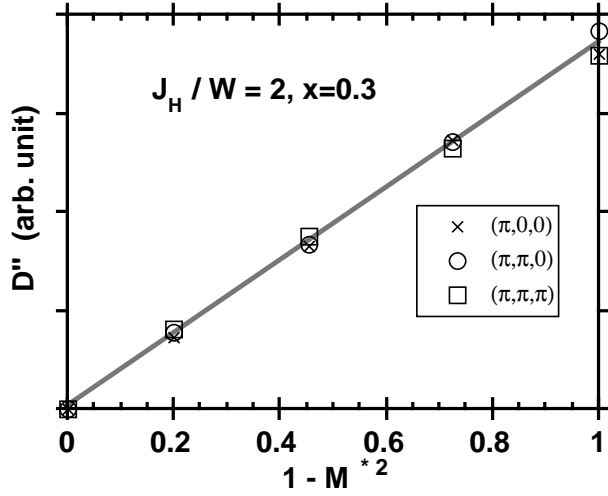


FIG. 3. Coefficient for ω -linear part $\partial \text{Im} \chi(Q, \omega) / \partial \omega |_{\omega \rightarrow 0}$ as a function of normalized magnetization M^* at various wave vectors. Line in the figure is a guide to eyes.

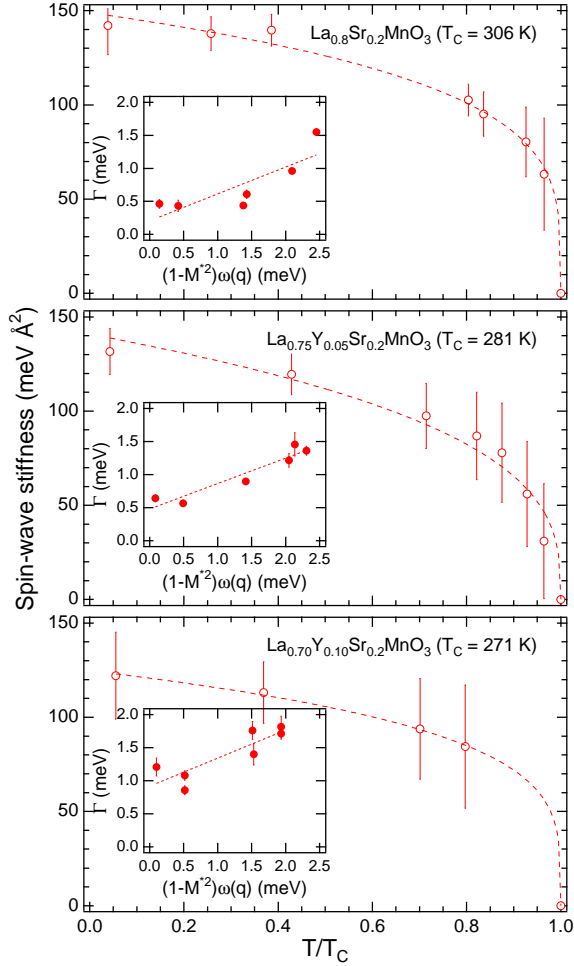


FIG. 4. Experimental results for the temperature dependence of the spin-wave stiffness D . Error bars indicate fitting errors. Dashed lines are guides to the eye. Inset shows a linear relation between $\Gamma(q, T)$ and $(1 - M^{*2})\omega(q, T)$, where $M^* = M(T)/M(0)$, at $q = (1.1, 1.1, 0)$ in rlu.

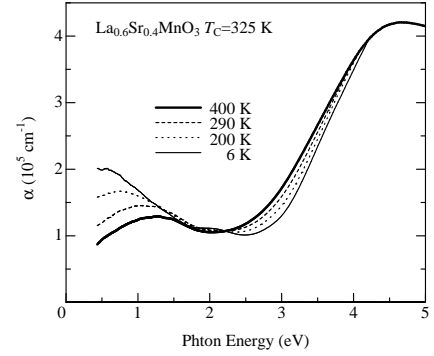


FIG. 5. Temperature dependence of absorption spectrum $\alpha(\omega)$ for $\text{La}_{0.4}\text{Sr}_{0.6}\text{MnO}_3$ film. The hatched area (α_{CT}) is due to the charge-transfer transition.

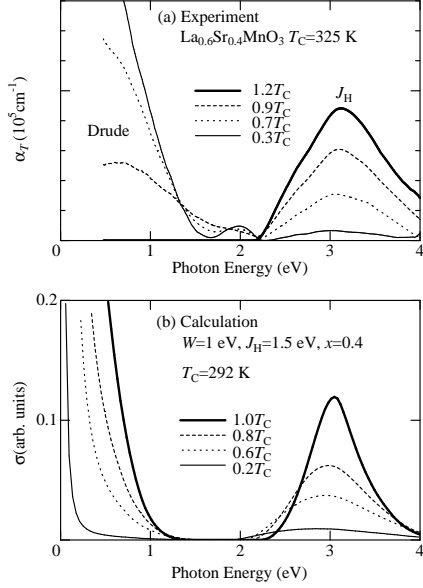


FIG. 6. (a) Temperature-dependent component of the absorption spectrum $\alpha_T(\omega)$ for $\text{La}_{0.6}\text{Sr}_{0.4}\text{MnO}_3$. The bands denoted by J_H is due to interband transition between the J_H -split bands. (b) Calculated results based on the double-exchange model with DMF and $S=\infty$ approximation. The used parameters are $W=1$ eV, $J_H=1.5$ eV and $x=0.4$.

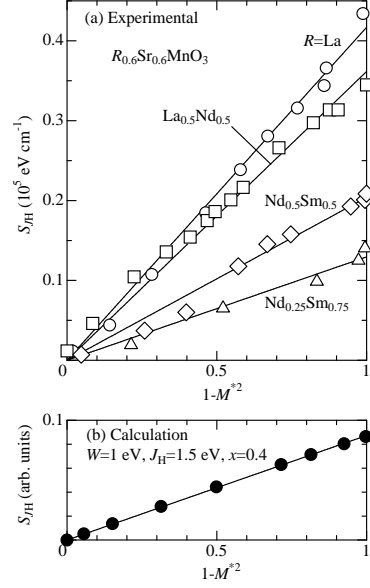


FIG. 7. (a) Spectral weight S_{J_H} of the J_H -gap transition against $1 - M^{*2}$, where $M^* = M(T)/M(0)$ is the magnetization normalized by its saturation value. (b) Calculated results based on the double-exchange model with DMF and $S = \infty$ approximation ($W=1$ eV, $J_H=1.5$ eV and $x=0.4$).